J Appl Electrochem (2007) 37:1303–1312
DOI 10.1007/s10800-007-9410-5

ORIGINAL PAPER

Potential and current density distributions along a bipolar electrode

R. Kodým · K. Bouzek · D. Šnita · J. Thonstad

Received: 7 March 2007 / Revised: 27 August 2007 / Accepted: 29 August 2007 / Published online: 26 September 2007

Abstract Potential and current density distributions were modelled and measured for an electrochemical cell with a bipolar electrode. The dimension of the bipolar electrode in the direction of current flow was extended, to enable experimental determination of the electrode potential and the local current densities at various positions inside the electrolyte and in the electrode body. The experimental results showed that the most active regions of the bipolar electrode are located at the ends of the bipolar electrode facing the terminal electrodes. The equations corresponding to the mathematical model of the experimental cell were solved using the finite volume method and gave very good qualitative agreement with the experimental data. However, some discrepancies between model predictions and experimental data were evident in the active parts of the bipolar electrode and in the variation of the terminal voltage with the total current. This was explained in terms of the active electrolyte cross-section and the electrode surface area being diminished due to the presence of gas bubbles in the system.

R. Kodým · K. Bouzek (✉)
Department of Inorganic Technology, Institute of Chemical Technology Prague, Technická 5, 166 28 Prague 6, Czech Republic
e-mail: karel.bouzek@vscht.cz

D. Šnita
Department of Chemical Engineering, Institute of Chemical Technology Prague, Technická 5, 166 28 Prague 6, Czech Republic

J. Thonstad
Department of Material Science and Engineering, Norwegian University of Science and Technology, 7034 Trondheim, Norway

Keywords Bipolar electrode · Mathematical modelling · Parasitic current · Local potential and current density distribution

Nomenclature

A_F	Cross-sectional area of the free electrolyte space beside the bipolar electrode (m^2)
d_G	Inter-electrode distance (m)
d_E	Bipolar electrode thickness (m)
E	Electrode potential (V)
f_E	Current utilisation in a bipolar cell (–)
I	Current (A)
I_E	Current flowing through bipolar electrode (A)
I_P	Parasitic current (A)
I_T	Total current (A)
j	Current density (A m^{-2})
n	Vector normal to the boundary (m)
N	Number of electrolytic cells (–)
r	Radius (m)
R	Resistivity (Ω)
R_F	Electrolyte resistivity in the fictitious electrolyser (Ω)
R_G	Average resistivity of the inter-electrode gap (Ω)
R_S	Short-circuit resistivity (Ω)
S	Electrode surface (m^2)
U	Voltage (V)
U_r	Open-circuit cell voltage (V)
x	Position along the cell (m)

Greek letters

φ	Galvani potential (V)
σ	Conductivity (S m^{-1})
κ_F	Electrolyte conductivity (S m^{-1})
η	Overpotential (V)

Subscripts

A	Anode
b	Boundary
C	Cathode
e	Electrode
l	Electrolyte
i	Cell number index

1 Introduction

Bipolar electrodes are widely used in technical practice, e.g. in brine [1] and water electrolysis [2] and magnesium production [3]. For aluminium production [4] several types of electrolytic cells have been proposed [5]. The main advantage of a bipolar arrangement is the simplified cell construction. The bipolar electrolyser requires the external current leads to be connected only to the two terminal electrodes, simplifying the electrical circuitry and enabling the electrolyser to be more compact. This arrangement is highly advantageous mainly for processes working either at high temperatures (magnesium and aluminium production, etc.) and/or at elevated pressure, such as water electrolysis. Another advantage of this electrolyser arrangement consists in the use of a lower current at higher voltage in comparison to monopolar cells, which is favourable in terms of the reduction of the ohmic drop on the current leads and efficiency increase of the rectifier.

However, the design of such systems has to meet the requirements associated with the supply, circulation and removal of solutions and products (including heat). Ionic conduction paths in solution beyond the inter-electrode gap lead to the existence of a so-called parasitic (also referred to as a bypass or shunt) current, i.e. current flowing between separate electrolytic cells outside the bipolar electrode assembly (e.g. through the manifolding system). This decreases apparent process current efficiency. Therefore, the control of such parasitic current is essential to the design of a bipolar cell.

An effective solution to these problems requires a more fundamental understanding of the related processes, as well as reliable mathematical models capable of optimising the stack design in order to minimise bypass currents. The magnitude of the bypass current can be calculated from the local Galvani potentials. Models of local potential distribution are generally based on the solution of the Laplace equation, Eq. 1, where φ is a Galvani potential and σ represents the conductivity of the medium.

$$\nabla(\sigma\nabla\varphi) = 0 \tag{1}$$

Nowadays the numerical solution of this equation is well understood for classical monopolar cell arrangements, see e.g. [6–8]. Generally, one of four well-established methods is used to accomplish this task: (1) Network of Linear Resistors (NLR); (2) Finite Differences Method (FDM); (3) Finite Elements Method (FEM) and (4) Boundary Elements Method (BEM). The NLR is based on the physical models used in the past [9]. The results represent a rough estimate of the real situation, and this method is used only rarely. The FDM is based on the replacement of the derivatives in the Laplace equation by finite difference formulae [4, 10]. The resulting system is usually solved iteratively using a relaxation method. FEM has several significant advantages over FDM: it approximates the curved boundaries with higher accuracy, and discretisation using FEM provides a set of algebraic equations, which can be solved directly [11]. The main advantage of BEM is that it reduces the dimensions of the problems, since the fundamental solution to the equation is known, it just needs to be solved at the boundaries [6, 8]. The selection of a suitable method to solve the problem is highly individual and depends on the system concerned. Generally, FEM has recently become the preferred method of calculating the field of the Galvani potential distribution.

In the case of the bipolar electrochemical cell geometry, two types of models can be distinguished. The first is characterised by separation of the individual electrochemical cells by an insulating barrier. Thus, the bypass current in such an arrangement flows only through the pipeline system [11–15]. These systems are characterised by relatively homogeneous current density distribution and by the absence of the anode–cathode transition region along the side of the bipolar electrode. Characteristic examples of such arrangements are industrial membrane brine or water electrolysers [2, 10, 13, 16, 17]. In such a case, the NLR method is sufficient to assess the parasitic current decreasing apparent process efficiencies. This is a classical approach and a series of papers have already been published in the literature [13]. In comparison to the NLR method, the FDM approach additionally enables detailed information to be obtained on the local Galvani potential distribution in the cell. A representative example is the work of Divisek et al. [10], who took advantage of the FDM to identify the zones of a bipolar cell stack that were endangered by corrosion.

Mathematical modelling of bipolar porous electrodes is a special case. Cheng et al. [18] developed a one-dimensional steady-state model for recovery of Pb(II) ions from the effluents of lead-acid battery recycling plants. Both monopolar and bipolar electrochemical cells with porous graphite electrodes were simulated. The model was implemented and the governing equations solved using commercial FEM software (FEMLAB). According to the model results, the bipolar construction was found to be inappropriate for the recovery of Pb(II) from the effluents due to a very high by-pass current of >90%.

Recently, Henquin and Bisang [19] proposed a simplified mathematical model of the current density distribution, enabling prediction of the effects of the geometry and operational variables on the current distributions at the bipolar and terminal electrodes. The important parameters were combined into two dimensionless parameters.

The second type of model is characterised by bipolar electrodes placed in an electrochemical cell, allowing parasitic current to flow directly inside the cell along their sides. One typical example is the electrochemical aluminium production unit designed and tested by Alcoa [4]. Modelling of this type of cell is significantly more complex. Therefore, originally an empirical approach was used to predict current efficiencies. A first attempt in this direction was undertaken by Ishikava and Konda [20]. They assumed that the electric current in a bipolar electrolyser can be divided into two parts: the first flows through all bipolar electrodes; the second flows directly from the terminal anode to the terminal cathode. Using this assumption, a fictitious electrolyser was introduced through which the parasitic current flows. The parasitic current can be calculated using Eq. 2,

$$I_p = \frac{(N-1)\cdot(U_r+\eta_A-\eta_C)+N\cdot R_G\cdot I_T}{R_F+N\cdot R_G} \tag{2}$$

where I_T is the total current flowing through the cell, I_P the parasitic current, U_r the open circuit cell voltage, $\eta_{A,C}$ the overvoltage of the anodic and cathodic reactions, respectively, at the electrodes, R_F the electrolyte resistivity in the fictitious electrolyser, R_G the average resistivity of the inter-electrode gap and N the number of electrolytic cells. Furthermore, they defined current efficiency or the "utilisation" of the current for the electrochemical process for bipolar cells used, as given by Eq. 3.

$$f_E = \frac{I_T+(N-1)\cdot(I_T-I_P)}{N\cdot I_T} \tag{3}$$

According to [21], the terminal electrodes and one half of the inter-electrode gaps adjacent to them, form a fictitious cell through which the total current flows. Each bipolar electrode with one half of the inter-electrode gap on each side, represents another fictitious cell, short-circuited by the resistor R_s.

$$R_s = \frac{1}{\kappa_F}\frac{(d_G+d_E)}{A_F}. \tag{4}$$

The symbols in Eq. 4 represent the following: κ_F—electrolyte conductivity; d_G, d_E—inter-electrode distance and bipolar electrode thickness, respectively; A_F—cross-sectional area of the free electrolyte space for short-circuiting the bipolar plate. The voltage balance for each bipolar electrode then reads:

$$I_{p,i} = \frac{V_{r,i}+\eta_{A,i}-\eta_{C,i}+R_G\cdot\left(I_T-I_{P,i}\right)}{R_S} \quad i=2,\ 3,\ \ldots,N. \tag{5}$$

Subscript i corresponds to the number of the related bipolar plate and $(N-1)$ is the total number of bipolar cells in the stack. For large values of N, the limiting values of current efficiencies calculated from Eqs. 3 and 5 are identical.

Comninellis et al. [22] estimated bypass currents for an electrolyser with up to 14 bipolar electrodes simply from the experimental current–potential (i–U) curves, measured for an one-element bipolar cell electrolyser. At high currents an acceptable agreement was obtained with the experimental data.

A more rigorous way was chosen by Roušar and Thonstad [4], who described the Alcoa cell for aluminium production from a molten salt containing aluminium chloride. This is the only study known to the authors that presents a solution of the Laplace equation in the entire model domain of the bipolar electrochemical cell, allowing for current flowing along the bipolar electrodes sides. The following condition was used to estimate the Galvani potential inside the graphite bipolar electrodes.

$$\oint j dS_i = 0 \quad i=2,\ 3,\ldots,N.$$

The numerical solution of the Laplace equation allowed a detailed description of the influence of the flow of bypass current on current density distribution. The FDM was used to solve the Laplace equation. The secondary current density distribution was provided using Tafel kinetics for chlorine evolution and molten aluminium deposition. It was considered that an electrode reaction can take place at a bipolar electrode, only if the ohmic potential losses at their sides exceed the equilibrium voltage of $AlCl_3$ decomposition. This means that the polarisation curve corresponding to the Alcoa process was partially simplified, enabling the convergence problems of the mathematical method to be solved. The results of their theoretical calculations were not proven experimentally, but were compared with the simplified bypass current calculations, presented by Ishikawa and Konda [20] and by Rousar [21]; reasonable agreement was obtained.

The aim of this paper is to present a method for solving Laplace's equation in a bipolar electrochemical cell without insulating barriers, and to validate the model's predictions by a comparison with experimental data.

2 Experimental

Figure 1 shows a schematic of the model cell, consisting of a rod placed concentrically in a cylindrical electrolyser, equipped with terminal electrodes at both ends. The rod acting as a bipolar electrode was 780 mm long and 3 mm in diameter. The terminal electrodes were of a cylindrical plates form, 1 mm thick, filling completely the electrolyser cross-section. The distance between each of the terminal electrodes and the bipolar electrode was 25 mm. Both the terminal electrodes and the bipolar electrode were made of smooth platinum. Cylindrical electrolysers of two different diameters, 8 and 14 mm, were used. The surface of the bipolar electrode was contacted at regular intervals via Pt wires, in order to record the ohmic Galvani potential drop within the bipolar electrode. The measurement of the ohmic drop was accomplished by means of a Microvoltmeter MT 100 (Metra Blansko, Czech Republic). Luggin capillary tips were placed close to the bipolar electrode surface in positions aligned with the contacting Pt wires. This made it possible to observe, parallel to the ohmic drop within the bipolar electrode, the Galvani potential field distribution in the electrolyte solution, together with local values of the bipolar electrode potential. A 0.5 M solution of HCl of analytical grade was used as the electrolyte. It was fed to the centre of the electrolyser, so that the flow was uniformly divided on both sides of the cell. The continuous flow of electrolyte during the experiments ensured removal of the electrode reaction products from the electrolyser.

The electrolyte flow rate was kept constant at 1.0 and 0.25 dm^3 min^{-1} for all experiments with cell diameters 14 and 8 mm, respectively. All experiments were performed under galvanostatic control.

Figure 2 shows a schematic of the electrolyser, with a twin concentric polymethylmethacrylate tubular body, used vertically for determination of the polarisation curve of platinum in a flowing electrolyte; it was designed to provide experimental conditions (flowing electrolyte, no anolyte and catholyte mixing) similar to those in the bipolar cell.

The bipolar Pt electrode was located in the centre of the inner tube and the counter electrode was placed between

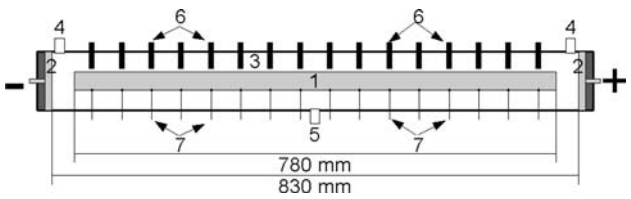

Fig. 1 Schematic of the experimental bipolar cell: 1—Pt rod, 2—terminal electrodes, 3—electrolyte, 4—outlets, 5—inlet, 6—Luggin capillary tips, 7—Pt wire contacts

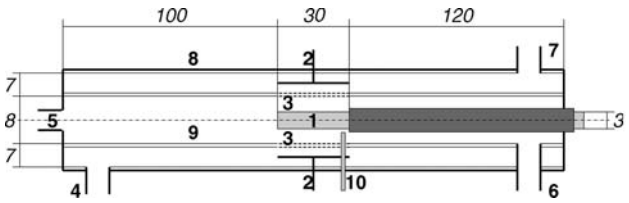

Fig. 2 Schematic of the cell used to determine the polarisation curve in flow-through mode: 1—Pt working electrode, 2—counter-electrode, 3—perforated tube, 4, 5—electrolyte inlets, 6, 7—electrolyte outlets, 8, 9—external and internal cell walls, respectively, 10—reference electrode (numbering in bold); for dimensions, see numbers in italics (in mm). The cell was operated vertically

the inner and outer tubes. Holes in the wall of the internal tube completed the electrical circuit between the working and the counter electrode, ensuring even current density distribution at the working electrode surface, but minimised mixing the anolyte and the catholyte. At a constant temperature of 22 °C, the electrolyte was fed at the bottom of the cell and left through the upper outlets at a constant flow rate of 0.25 dm^3 min^{-1}. A saturated calomel reference electrode (SCE) was used, although potential values in the text are quoted against the SHE electrode, assuming the electrode potential of an SCE is +0.245 V (SHE).

3 Mathematical model description

A mathematical model was developed, describing the secondary local potential and current density distribution in the bipolar electrolysers described above. The electric current distribution was calculated using cylindrical coordinates in a two-dimensional cross-section of half of the cell, as shown in Fig. 3, in which r represents the perimeter and x a position along the electrolyser. The grey areas indicate the domain of electrodes and the white space represents the electrolyte domain. This simplification is possible because of the electrolyser's symmetry.

3.1 Boundary conditions

The electrolyser wall ($r = r_2$ and $x \in \langle 0,\ x_5 \rangle$) was treated as an insulator. In the centre of the cell ($r = 0$ and $x \in \langle 0,\ x_5 \rangle$) a symmetrical boundary condition was applied. For both insulation and symmetrical boundary conditions,

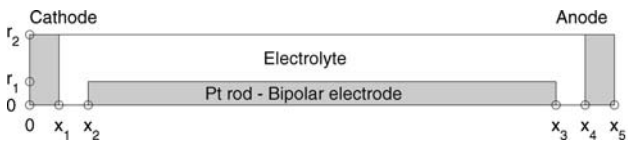

Fig. 3 Schematic of the bipolar cell model

zero potential gradients in the direction normal to the boundary were considered:

$$\frac{\partial \varphi}{\partial n} = 0 \tag{7}$$

At the surface of the bipolar electrode ($x \in \langle x_2, x_3 \rangle$, $r = r_1$; $x = x_2$ and $x = x_3$, $r \in \langle 0, r_1 \rangle$), the continuity of the electric current flux expressed by:

$$j_{eb} = j_{bl} = j_b, \quad j_{eb} = -\sigma_e \left.\frac{\partial \varphi}{\partial n}\right|_{eb}, \quad j_{bl} = -\sigma_l \left.\frac{\partial \varphi}{\partial n}\right|_{bl} \tag{8}$$

is considered, where j_{eb} is the current density in the electrode in the direction normal to the electrode/electrolyte interface, j_{bl} is the current density in the electrolyte in the direction normal to the electrode/electrolyte interface (the normal orientation is from the electrode to the electrolyte), j_b is the intensity of the electric current from the electrode to the electrolyte in the normal direction to the interface, σ_e corresponds to the electronic conductivity of the electrode, σ_l is the ionic conductivity of the electrolyte, $\left.\frac{\partial \varphi}{\partial n}\right|_{eb}$ is the normal derivative of the electric potential in the electrode at the electrode/electrolyte interface and $\left.\frac{\partial \varphi}{\partial n}\right|_{bl}$ is then the normal derivative of the electric potential in the electrolyte at the electrode/electrolyte interface.

At the same time the Galvani potential is discontinuous at the electrode/solution interface, since:

$$\varphi_{eb} = \varphi_{bl} + E_b \tag{9}$$

where φ_{eb} represents the Galvani potential in the electrode at the electrode/electrolyte interface, φ_{bl} is then the Galvani potential in the electrolyte at the electrode/electrolyte interface, E_b indicates the electric potential drop across the electrode/electrolyte interface, i.e. the electrode potential. The current density and the electrode potential are coupled by the equation describing the electrode reaction kinetics:

$$j_b = j(E_b) = f(\varphi_{eb} - \varphi_{bl}) \tag{10}$$

In the present case, where an equilibrium electrode potential is not defined, the empirical polarisation curve based on the fitting of the experimental points by an empirical exponential function was used:

$$\begin{aligned} j &= B(e^{-K_1*(E-U_1)} + e^{-K_2*(E-U_2)} - C); \\ C &= e^{-K_1*(A-U_1)} + e^{-K_2*(A-U_2)} \end{aligned} \tag{11}$$

The interface between both terminal electrodes and the electrolyte was described in the same way. Therefore, subscripts are not used for j and E. Finally, a non-zero constant Galvani potential was applied at the boundary ($x = x_5$ and $r \in \langle 0, r_2 \rangle$) for the anode and equal to zero for the cathode ($x = 0$ and $r \in \langle 0, r_2 \rangle$).

3.2 Method of solving the model equations

A rectangular non-equidistant spatial grid was used for the numerical approximation of the differential equations by the finite volume method. The system of the linear algebraic equations was obtained from the Laplace equation, formulated in cylindrical coordinates both in the electrode domain and in the electrolyte domain. After the numerical approximation of boundary condition (8), an additional set of linear algebraic equations was obtained. On the other hand, the numerical approximation of the boundary condition (10) gave a second additional set of non-linear algebraic equations. The full system of equations was solved by means of Newton's method using MATLAB™ (http://www.mathworks.com). The first calculation was performed for the trivial case of zero current, which was gradually increased subsequently. The Galvani potential field calculated in one step was used as an initial guess in the subsequent calculation, ensuring numerical stability of the iterations.

3.3 Input parameters

The cell dimensions used for the calculation are as follows: r_1 = 1.5 mm; r_2 = 7.0 mm (or 4.0 mm); x_1 = 30 mm; x_2 = 55 mm; x_3 = 835 mm, x_4 = 860 mm and x_5 = 890 mm. Conductivity values of 17 S m^{-1} (Lobo [23]) and 8.40×10^6 S m^{-1} [24] were used for the electrolyte and Pt, respectively. Figure 3 explains the meaning of the individual symbols.

4 Results and discussion

4.1 Polarisation curve of a Pt electrode in the flow-through system

Figure 4 shows the experimental polarisation curve of a platinum electrode in 0.5 M HCl pumped in single pass flow-through mode; together with the empirically fitted polarisation curve (Eq. 11). The following numerical parameters values were obtained for a current density range of ±80 mA cm^{-2}: K_1 = 0.03 mV^{-1}, K_2 = 0.03 mV^{-1}, U_1 = –200 mV, U_2 =970 mV, A = 400 mV and B = 0.1 mA cm^{-2}. Equation 11 then matched the experimental data well at higher current densities, but there was a minor discrepancy for current densities close to zero, where an additional mass transfer limited reaction seemed to appear at a potential of approx. 30 mV. It is highly probable that this corresponded to reduction of the oxygen dissolved in the electrolyte.

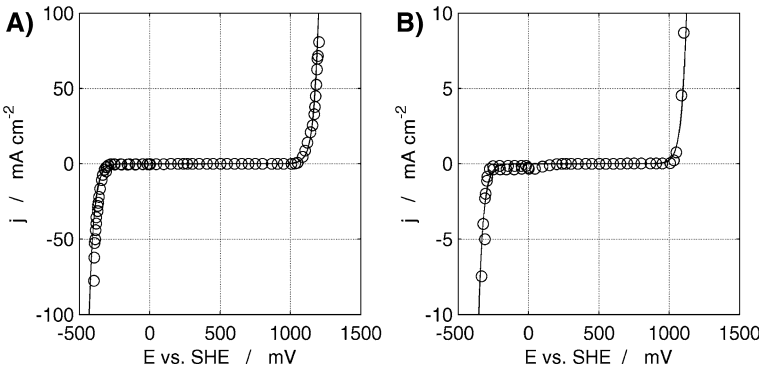

Fig. 4 Polarisation curve; points represent experimental data, lines the fitted polarisation curve, see Eq. 11; **A**—overall curve, **B**—scaled mixed electrode potential region of the polarisation curve

4.2 Experimentally determined local potential and current density distribution along the bipolar electrode

Local potential and current density distributions were determined for the two different electrolyser cross-section areas and for currents of 5–60 mA. Figure 5A shows the resulting dependence of the local bipolar electrode potentials on current. The current flowing through the bipolar electrode was determined by establishing the local ohmic potential drop along it. The data obtained were transformed into dimensionless form by dividing them by the total cell current as shown in Fig. 5B. As expected, in the middle region of the bipolar electrode, these experimental results showed a linear dependence of the electrode potential on position. This confirms the electrochemical inactivity of the electrode in this section. In agreement with this observation, the current flowing through the bipolar electrode remained practically independent of the position in this domain, except for the two lowest currents used. The accuracy of these data was limited to ±20%, as the current was evaluated from the measured ohmic potential drop resulting from electric currents of units of milliamperes passing through the Pt rod of 3 mm diameter.

At the ends of the bipolar electrode, regions of electrochemical activity were clearly evident, characterised by a change in the dependence of the bipolar electrode potential on position from linear to exponential (see Fig. 5A). At the same time, the electrical current flowing through the body of the bipolar electrode decreased, as shown in Fig. 5B. One interesting feature is the asymmetry in the electrochemically active part of the electrode, which is more pronounced on the cathodic side of the bipolar electrode in the lower current density range (≤20 mA), as discussed below.

With respect to the different diameters of the electrolyser (14 and 8 mm), no significant qualitative differences in current density and local bipolar electrode potential distribution were detected experimentally.

4.3 Mathematical model results

The local Galvani potential distribution was calculated using the mathematical model described in Sect. 3; an example of the result is given in Fig. 6. The slope of the Galvani potential decreased within the electrolyte in the direction from the anode to the cathode and reached the highest value in the area between the terminal electrodes and the edge of the bipolar electrode. This was because the current flowed solely through the electrolyte in this domain. At the coordinates of the edge of the bipolar electrode, the gradient changed and the decrease is much less rapid, due to part of the current flowing through the bipolar electrode.

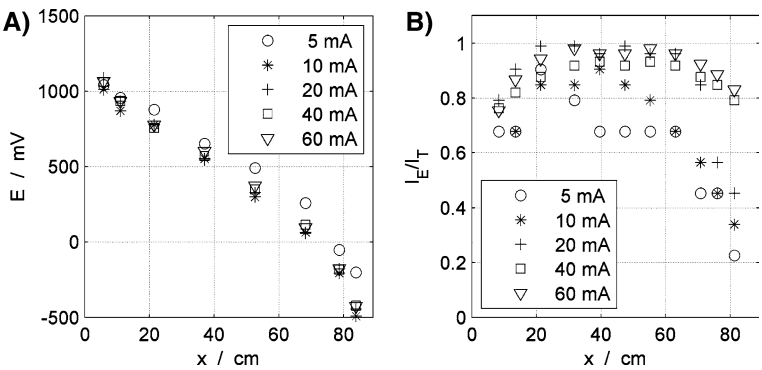

Fig. 5 Experimentally determined (**A**) electrode potential distribution along the bipolar electrode, and (**B**) the fraction of the electrical current flowing through the bipolar electrode body for different currents, the values in the graph inset indicate the cell current—I_T, electrolyte—0.5 M HCl, flow rate—0.25 dm^3 min^{-1}, electrolyser diameter—14 mm

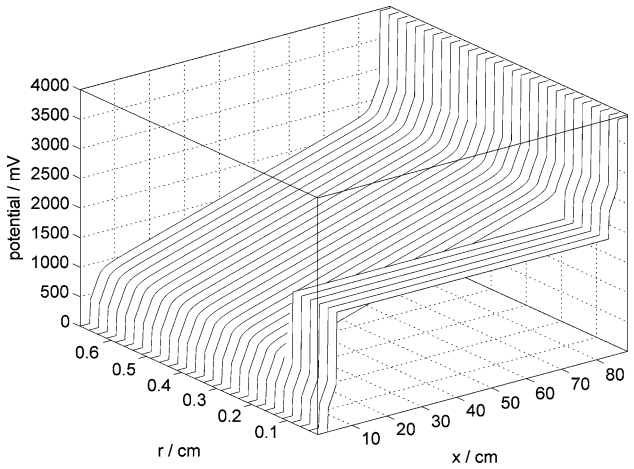

Fig. 6 Calculated secondary Galvani potential distribution in a bipolar cell (current 40 mA; cell voltage 4.0 V), electrolyte conductivity—17 S m^{-1} and electrolyser diameter –14 mm

This is more clearly demonstrated in Fig. 7, showing the calculated current flow-lines in the cross-section of the cell. As observed for the experimental data, these figures show similar trends, and the explanation given for Fig. 5A and B also applies in the present case. This provides additional information about the distribution of the current flow paths in the bulk of the electrolyte and clearly documents the phenomenon discussed for the local Galvani potential field shown in Fig. 6. In agreement with other results, it demonstrates that an increasing portion of the bipolar electrode became active with increasing current/potential drop in the electrolyte.

Local values of the bipolar electrode potentials and current densities were calculated using the Galvani potential field resulting from the mathematical model. The calculated dependence of the bipolar electrode potential on position is given in Fig. 8A. Figure 8B shows the calculated local values of the part of the total current flowing through the inside of the bipolar electrode. The results are in good qualitative agreement with the experimental data shown in Fig. 5, except for the distribution of the active parts of the bipolar electrode, as discussed later.

The observed and calculated dependences of the bipolar electrode potential on position, shown in Figs. 5A and 8A, as well as the electric current flowing through the body of the bipolar electrode, as seen in Figs. 5B and 8B, corresponded well with the general theory of bipolar electrodes. The highest current densities through the bipolar electrode/electrolyte interface and the exponential changes in the potential of the bipolar electrode with the position, were observed at both ends close to the terminal electrodes. Conversely, almost negligible electrochemical activity and also the highest current flowing through the body of the bipolar electrode, were observed in the central region of the electrode. This was due to the Galvani potential differences between the bipolar electrode and the electrolyte solution being lower in this region than the potential necessary to overcome the activation barrier of the particular electrode reaction. Since the conductivity of Pt is six orders of magnitude higher than that of the electrolyte, the ohmic potential drop within the bipolar electrode can be neglected. Thus, the most significant changes in the bipolar electrode potential have to be expected at its electrochemically active ends. With increasing total cell current, both active regions of the bipolar electrode increased, due to the higher ohmic potential drop in the electrolyte and hence greater potential

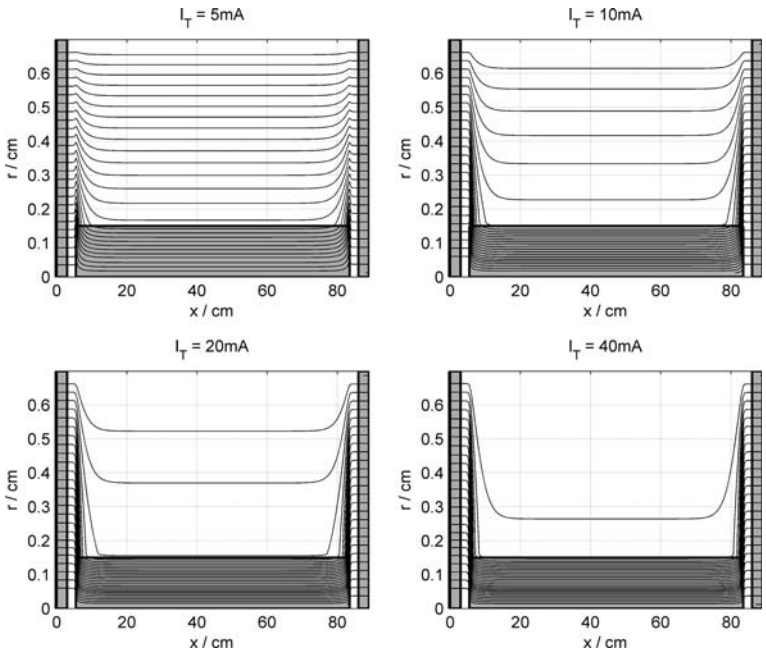

Fig. 7 Current flow-lines of the entire electrolyser for various currents, indicated above the individual figures, cell voltage—2.7 V (5 mA), 3.0 V (10 mA), 3.2 V (20 mA), 4.0 V (40 mA); electrolyte conductivity—17 S m^{-1}, electrolyser diameter—14 mm

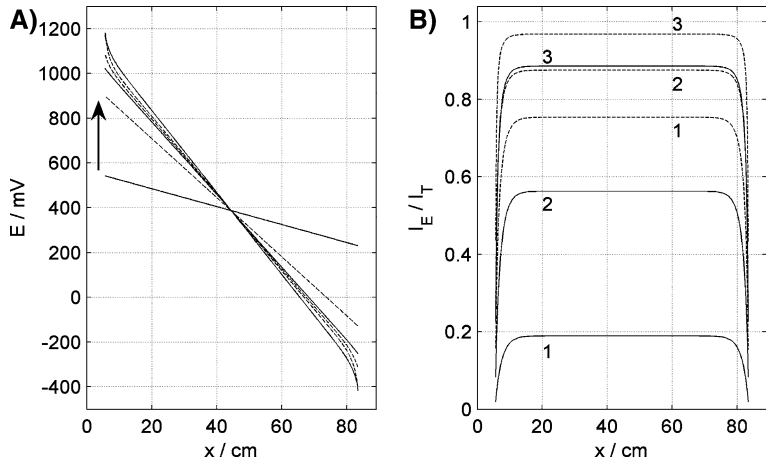

Fig. 8 Calculated values of (**A**) electrode potential distribution along the bipolar electrode, and (**B**) the fraction of the electrical current flowing through the bipolar electrode body for different currents and different electrolyser diameters; (**A**) dotted line: electrolyser diameter—8 mm, solid line: electrolyser diameter—14 mm, the arrow indicates the direction of increasing total current (1, 5, and 40 mA); (**B**) currents of: (1)—5 mA, (2)—10 mA, (3)—40 mA, dashed line and numbers on the right side: electrolyser diameter—8 mm, solid line and numbers on the left side: electrolyser diameter—14 mm; electrolyte conductivity—17 S m^{-1}

difference between electrode and solution phases, leading to greater reaction rates on the bipolar electrode. The almost ideal symmetry of the anodic and cathodic reactions on the bipolar electrode predicted by the mathematical model corresponds to the symmetry of the polarisation curve used.

The dependence of cell voltage on the current in Fig. 9A shows, as expected, two main regions of behaviour for the two cell diameters used. At ca. <2.8 V, the bipolar electrode was inactive and the increase in cell voltage with current was caused by the two overpotentials and the potential ohmic drop in the electrolyte phase, the smaller active cross-section for the 8 mm diameter cell, the voltage increase is steeper. At cell voltages ca. >2.8 V, the bipolar electrode became active and the gradient of the *U–I* relationship decreased significantly, the voltage again increasing more rapidly with current for the 8 mm diameter cell, due to its smaller active cross-section.

As expected, Fig. 9B indicates that a larger Galvani potential difference (ΔE) was needed over the entire bipolar electrode length (curve 1) for the 8 mm diameter cell to pass the same current as in the 14 mm diameter cell. This was due to the smaller active cross-section of the cell and thus higher portion of the total current flowing through the bipolar electrode. Higher Galvani potential differences along the bipolar electrode correspond to higher driving forces needed to overcome kinetic barriers of the electrode reactions on its ends. Surprisingly, in the middle region of the bipolar electrode (curve 2), the situation was different. For currents higher than ca. 6 mA, i.e. after bipolar electrode activation, the potential difference was higher

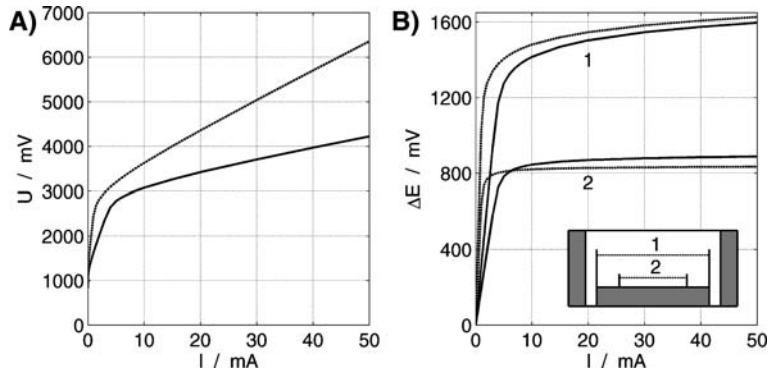

Fig. 9 Effect of total current on (**A**) cell voltage (*U*) for electrolyser diameter of 14 mm (solid line) and diameter 8 mm (dotted line), respectively; (**B**) bipolar electrode potential difference between two points along the bipolar electrode, for two different cases, as indicated in the schematic diagram inside **B** (corresponding to Fig. 3); distance of the points for the curve 1 = 780 mm (i.e. entire bipolar electrode length), for the curve 2 = 480 mm (i.e. prevailing electrochemically inactive part in the centre of the bipolar electrode); diameter 14 mm (solid line) and diameter 8 mm (dotted line); electrolyte conductivity—17 S m^{-1}

for the 14 mm diameter cell, because of the non-linearity of the polarisation curve, especially at higher current densities, and the two-dimensionality of the model. In agreement with reality, the electrolyser of diameter 14 mm allowed the current lines to spread more into the electrolyte space; in that case, current lines from the boundary of the terminal electrodes reached the active bipolar electrode surface at larger distance from its edge when compared with the cell of diameter 8 mm. This effect resulted in a larger Galvani potential difference in the centre of the larger diameter cell, even though its active cross-section was larger and the portion of the total current flowing through the bipolar electrode was significantly smaller, as shown in Fig. 8B.

Figure 10 shows the effect of cell current on the overall current utilisation in the bipolar electrode for both calculated and experimentally determined values, which increased rapidly with increasing cell current and reached unity for an infinitely high total current. By comparison, the mathematical model underestimates the enhancement in efficiency observed experimentally. The reason is clearly the presence of the gaseous phase in the cell, which was neglected in the mathematical model. The decrease in effective electrolyte conductivity due to the presence of the gas phase resulted in a significant increase in ohmic potential drop in the electrolyte and hence a higher portion of the current flowing through the bipolar electrode, i.e. enhanced bipolar electrode efficiency.

4.4 Parametric study of the influence of effective electrolyte conductivity

The explanation for the discrepancy between the experimentally determined and the calculated bipolar electrode efficiencies, was confirmed by the dependence of the total current on cell voltage, as shown in Fig. 11. At low currents, characterised by an exponential increase in current with cell voltage, increased overpotentials at both the bipolar and the terminal electrodes were largely responsible for the increase in cell voltage, whereas at higher currents, the ohmic potential drop in the electrolyte dominated the overpotential contributions, resulting in a linear increase of cell voltage with total current.

The results of the mathematical model were in good agreement with the experimental data in the low current region, when the gas fraction in the electrolyte was low, so had negligible effects. An attempt was made to improve the agreement between model predictions and experimental data by arbitrarily decreasing the input value of the electrolyte conductivity in the mathematical model; selected results are shown in Fig. 11. Even though those predicted results for an electrolyte conductivity of 0.034 S m^{-1} were relatively close to the experimental data, quantitative agreement was not achieved. This was due firstly to the local decrease in electrolyte conductivity depended on the local current producing bubbles, so that decrease was predominantly in the region between the terminal electrodes and the ends of the bipolar electrode, whereas such

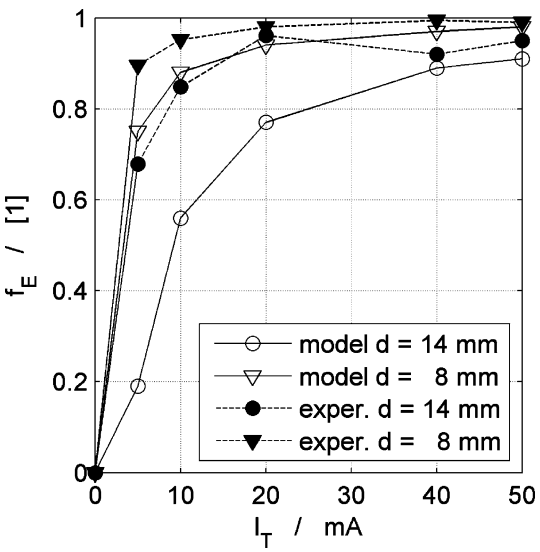

Fig. 10 Effect of total current on bipolar electrode efficiencies for different electrolyser diameters (14 and 8 mm), comparing experimental and mathematical model results; electrolyte—0.5 M HCl, flow rate—1.0 dm^3 min^{-1} (electrolyser diameter 14 mm) and 0.25 dm^3 min^{-1} (electrolyser diameter 8 mm), electrolyte conductivity—17 S m^{-1}

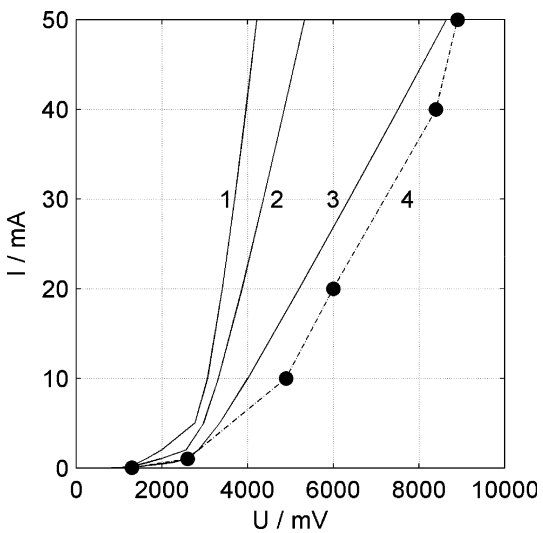

Fig. 11 Comparison of calculated (1–3) and experimental (4) values of the total current versus the terminal voltage; parametric study of the influence of the electrolyte conductivity: (1) 17.0 S m^{-1}, (2) 8.5 S m^{-1}, (3) 3.4 S m^{-1}; (4) electrolyte—0.5 M HCl (conductivity—17.0 S m^{-1}), flow rate—0.25 dm^3 min^{-1}, electrolyser diameter—14 mm

local variations were neglected in the model calculations. Secondly, for a certain time, the gas bubbles grew at the surface of the electrodes, especially at the edges of the bipolar electrode, decreasing the effective electrode surface, so that local current densities at the unshielded surface increased. The resulting increase in overpotentials caused the active part of the bipolar electrode to increase. This hypothesis was supported by the experimental data, which indicated that the active domains of the bipolar electrode were substantially larger than those resulting from the mathematical model calculations. Moreover, the active area of the cathodic part of the bipolar electrode was significantly larger than that of the anodic part, due to the solubility of the evolved chlorine being approximately by two orders of magnitude higher than those of hydrogen [25]. At high currents, the gas evolution rates on both ends of the bipolar electrode increased rapidly. Thus, solubility did not play an important role anymore. Moreover, due to the intensive electrolyte convection along the bipolar electrode surface causing detachment of bubbles, their coverage of the bipolar electrode surface became similar at both its ends, so the extent of the asymmetry in its cathodic and anodic areas became insignificant.

The gas evolved on the bipolar electrode plays a more significant role in the overall cell characteristics than the gas evolved at the terminal electrodes, as the bubbles were removed quickly from the surface of the terminal electrodes, through the cell outlet located in its vicinity. The gas evolved on the bipolar electrode had first to be transported by electrolyte convection along the bipolar electrode and through the space between the terminal and bipolar electrode on its way to the outlet.

5 Conclusions

The local electrode potential and current density distributions along and inside a bipolar electrode were modelled, the results being in agreement with the theory of the function of bipolar electrodes.

For the first time, the Laplace equation was solved, using the finite volume method, in a space representing the model structure of an experimental bipolar cell. The polarisation curve determined experimentally was used as a boundary condition on the surface of the electrode. Good qualitative agreement was obtained between the model results and the experimental data. The main discrepancies, at high currents, were caused by lower local effective electrolyte conductivities and by gas bubbles blocking part of the bipolar electrode surface. The solution to these problems will be the subject of further studies.

Acknowledgements Financial support of this research by the Grant Agency of the Czech Republic under Project No.: 104/05/066 and by the Ministry of Education, Youth and Sports of the Czech Republic under Project No. CEZ: MSM6046137301 is gratefully acknowledged.

Reference

1. White RE, Burney HS, Beaver RN (1986) Modern chlor-alkali technology. Ellis Horwood, Chichester (UK), p 365
2. Divisek J, Steffen B, Schmitz H (1994) Int J Hydrogen Energy 579:586
3. Sivilotti OG, Vandermeulen M, Iseki J (1996) Patent WO: 9633297 24th Oct
4. Roušar I, Thonstad J (1994) J Appl Electrochem 1124:1132
5. LaCamera AF (1987) Mathematical modelling of materials processing operations, TMS-AIME extractive and process metallurgy fall meeting, Palm Springs, CA, 29 Nov.–2 Dec. 1987, pp 671–691. The Metallurgical Society/AIME, Warrendale, PA, USA
6. Lapidus L, Pinder GF (1999) Numerical solution of partial differential equations in science and engineering. Wiley, New York (US), p 34
7. Britz D (1980) Digital simulation in electrochemistry. Springer, Berlin
8. Rousar I, Micka K, Kimla A (1986) Electrochemical engineering. ACADEMIA, Prague
9. King CJH, Danly DE (1982) J Electrochem Soc C118:C118
10. Divisek J, Jung R, Britz D (1990) J Appl Electrochem 186:195
11. Holmes J, White RE (1984) Electrochemical cell design. Plenum, New York
12. Froidevaux H, Mitha R, Salamin JY (1995) Chimia 3:12
13. White RE, Walton CW, Burney HS, Beaver RN (1986) J Electrochem Soc 133:485
14. Rangarajan SK, Yegnanarayanan V (1997) Electrochim Acta 153:165
15. Burnett JC, Danly DE (1979) Current bypass in electrochemical cell assemblies. AIChE Symp Ser 8:13
16. Divisek J, Mergel J, Schmitz H (1990) Int J Hydrogen Energy 105:114
17. Divisek J, Steffen B (1993) Calculation of the potential field, heat and mass distribution in a zero gap bipolar electrolyzer. In: Proc. Electrochem. Soc., vol 297. Electrochem. Soc., New Jersey, p 309
18. Cheng CY, Kelsall GH, Pilone D (2005) J Appl Electrochem 1191:1202
19. Henquin ER, Bisang JM (2005) J Appl Electrochem 1183:1190
20. Ishikawa T, Konda S (1983) Evaluation of bipolar electrode cell for electrowinning of liquid aluminium from chloride melts. In: Proc. 1st Inter. Symp. Molten Salts Chem. Technol. Kyoto, Apr. 20–22 B-102, 5:8
21. Rousar I (1969) J Electrochem Soc 676:683
22. Comninellis Ch, Plattner E, Bolomey P (1991) J Appl Electrochem 415:418
23. Lobo VMM (1989) Handbook of electrolyte solutions. Elsevier, Amsterdam
24. Linde DR (2006) Handbook of chemistry and physics, 87th edn. CRC Press, Boca Raton, pp 12–39
25. Seidell A (1940) Solubilities of inorganic and metal organic compounds, 3rd edn. D. Van Nostrand Company, New York